


Article

Enhanced Removal of Doxycycline by Simultaneous Potassium Ferrate(VI) and Montmorillonite: Reaction Mechanism and Synergistic Effect

Hangli Zhang¹, Shujuan Wang², Ji Shu³  and Hongyu Wang^{3,*}

¹ College of Civil Engineering and Architecture, Zhejiang Tongji Vocational College of Science and Technology, Hangzhou 311231, China

² College of Civil Engineering and Architecture, Zhejiang University of Technology, Hangzhou 310014, China

³ College of Environment, Zhejiang University of Technology, Hangzhou 310014, China

* Correspondence: hywang@zjut.edu.cn

Abstract: Doxycycline (DOX), a typical antibiotic, is harmful to aquatic ecosystems and human health. This study presents DOX removal by potassium ferrate (Fe(VI)) and montmorillonite and investigates the effect of Fe(VI) dosage, reaction time, initial pH value, montmorillonite dosage, adsorption pH, time and temperature on DOX removal. The results show that DOX removal increases when increasing the Fe(VI) dosage, with the optimal condition for DOX removal (~97%) by Fe(VI) observed under a molar ratio ([Fe(VI)]:[DOX]) of 30:1 at pH 7. The reaction of DOX with Fe(VI) obeyed second-order kinetics with a rate constant of $10.7 \pm 0.45 \text{ M}^{-1} \text{ s}^{-1}$ at pH 7. The limited promotion (~4%) of DOX adsorption by montmorillonite was observed when the temperature increased and the pH decreased. Moreover, the synergetic effect of Fe(VI) and montmorillonite on DOX removal was obtained when comparing the various types of dosing sequences (Fe(VI) oxidation first and then adsorption; adsorption first and then Fe(VI) oxidation; simultaneous oxidation and adsorption). The best synergistic effect of DOX removal (97%) was observed under the simultaneous addition of Fe(VI) and montmorillonite, maintaining the Fe(VI) dosage (from 30:1 to 5:1). Five intermediates were detected during DOX degradation, and a plausible DOX degradation pathway was proposed.

Keywords: advanced oxidation; potassium ferrate(VI); doxycycline degradation; synergistic reaction mechanism



Citation: Zhang, H.; Wang, S.; Shu, J.; Wang, H. Enhanced Removal of Doxycycline by Simultaneous Potassium Ferrate(VI) and Montmorillonite: Reaction Mechanism and Synergistic Effect. *Water* **2023**, *15*, 1758. <https://doi.org/10.3390/w15091758>

Academic Editors: Cassan Hodaifa, Antonio Zuorro, Joaquín R. Dominguez, Juan García Rodríguez, José A. Peres, Zacharias Frontistis and Mha Albqmi

Received: 26 February 2023

Revised: 28 April 2023

Accepted: 1 May 2023

Published: 3 May 2023



Copyright: © 2023 by the authors. Licensee MDPI, Basel, Switzerland. This article is an open access article distributed under the terms and conditions of the Creative Commons Attribution (CC BY) license (<https://creativecommons.org/licenses/by/4.0/>).

1. Introduction

The use of drugs and personal care products (PPCPs) as emerging contaminants has attracted extensive attention from around the world [1]. The “pseudo-durability” of antibiotics caused by the large-scale use of antibiotics in human, veterinary, agricultural and aquaculture activities [2], as well as the residual and continuous testing of antibiotics in the environment, have also attracted widespread concern [3–5]. Doxycycline (DOX), as one of the most important antibiotics, has been widely used and transferred to the aquatic environment, resulting in a high concentration in pharmaceutical wastewater, ranging from 3.9 ng/L to 500.0 µg/L [6–9]. Studies have also indicated that residual DOX in water threatens aquatic ecosystems and human health in the form of endocrine infections, as well as promoting bacterial resistance [10]. Therefore, the remediation of DOX is urgent.

Ferrate(VI) (Fe(VI)), a green and environmentally friendly agent, has multiple functions, such as oxidation, flocculation and adsorption, leading to its increasing use in water treatment. Wang et al. conducted a study of the mechanism of fluoroquinolone antibiotic and sulfonamides degradation by Fe(VI), which revealed the reaction rate constant for the fluoroquinolone reaction with Fe(VI) [11,12]. Su et al. focused on the trimethoprim and carbamazepine degradation by Fe(VI) and proposed a degradation pathway [13]. Yunho et al. assessed a technology for enhancing the dual functions of Fe(VI) to oxidize micropollutants

by the formation of ferric phosphates [14]. However, its redox potential decreases from +2.2 to +0.7 V when the environmental pH turns from acid to alkaline [13,15]. This results in the inefficient mineralization of target contaminations, leaving potentially toxic small molecular substances. For this reason, novel technology must be introduced to account for these limitations.

Adsorption technology plays an important role in wastewater treatment. The most important factor of adsorption between adsorbents and adsorbates is their hydrophobic and electrostatic interaction [16]. Montmorillonite, as a natural silicate mineral, has a relatively large specific surface area (SSA), with a high cation exchange capacity (CEC), which can be used as an efficient adsorption agent [17]. Therefore, the addition of montmorillonite may be an effective approach to the adsorptive removal of small molecular substances stemming from Fe(VI) degradation. Furthermore, montmorillonite can not only adsorb target pollutants in solution, but can also enhance the overall adsorption and flocculation capability of Fe(VI) by activating adsorption bridging, net flapping and sweeping and electrical neutralization with in situ Fe(III) particles from Fe(VI) decomposition.

This work's objectives were to: (i) explore the degradation performance of Fe(VI) by assessing the oxidation efficiency and mineralization of DOX; (ii) investigate the adsorption performance of DOX by montmorillonite; (iii) elucidate the mechanism of the synergistic effect of the oxidation and adsorption of DOX by Fe(VI) and montmorillonite; and (iv) identify the degradation products of DOX and propose a degradation pathway for DOX, considering the molecular structure of target pollutants and the oxidation mechanism of Fe(VI).

2. Materials and Methods

2.1. Chemicals and Materials

Doxycycline (DOX) with a purity of 98% and montmorillonite with a purity of over 95% were purchased from Aladdin (Shanghai, China). Fe(VI) was prepared by electrochemical methods with a purity of at least 90% [18]. Other chemical reagents were of analytical grade, purchased at Xiaoshan Chemical Reagent Factory (Hangzhou, China). All chemical solutions were prepared in Milli-Q water, with the initial concentration of DOX being 11.25 μM . The Fe(VI) stock solution was prepared in a borate buffer solution composed of 81% 0.05 M borax and 19% 0.2 M boric acid, with a pH of 9.2.

2.2. DOX Removal by Fe(VI)

In this study, the Fe(VI) concentration was determined by ABTS methods and detailed information is given in Text S1 [19]. Subsequently, a 1.0 mM Fe(VI) stock solution was prepared in borate buffer solution at pH 9.1 prior to the experiment. A total of 50 mL of 11.25 μM DOX was dispensed into a beaker and stirred using a magnetic stirrer (Thermo Scientific, MA, USA) at 200 rpm. The pH of the solution was adjusted using 0.1 M hydrochloric acid and 0.05 M sodium hydroxide to various levels, ranging from 4.0 to 10.0. Subsequently, various volumes of a 1 mM Fe(VI) stock solution were introduced to the reaction to maintain an initial Fe(VI) concentration range of 56.25 to 337.50 μM . At predetermined intervals, samples were collected, the reaction was quenched with 30.0 μL of 0.1 M sodium thiosulfate and filtered through a 0.22 μm membrane filter (Xingya, Shanghai, China). These samples were further used to quantify the residual DOX concentration and total organic carbon (TOC), to determine the DOX removal efficiency and mineralization. To exclude the effect of filtering, the recovery rate after filtering was measured (Figure S1). The result showed that the recovery rate was close to 100% with various initial DOX concentration injections, indicating that the filtering process did not affect the subsequent experiments.

2.3. DOX Removal by Montmorillonite Adsorption

Before the experiment, 50 mL of 11.25 μM DOX was added to a beaker. The pH of the solution was adjusted, as described in Section 2.2. Subsequently, the solution was supplemented with montmorillonite powder. The mixture was then stirred using a

magnetic stirrer (IKA, Schwarzwald, Germany) at 250 rpm, at a temperature of 25 °C. After 24 h of adsorption, the supernatant was withdrawn and centrifuged at 200 rpm for 10 min. The centrifuged sample was then filtered through a 0.22 µm membrane filter (MF-Millipore, Hongkong, China), to determine the DOX concentration.

2.4. Kinetics Study

The reaction kinetics of Fe(VI) with DOX were investigated at 20 °C under pseudo-order conditions, with an excess Fe(VI) concentration of [Fe(VI)]:[DOX] = 49.8:1 to 199.2:1 at pH 7.0. The initial concentration of DOX was 2.25 µM. Samples were taken from the mixture at pre-determined time intervals, up to 1800 s, and then immediately quenched with 30.0 µL of a 0.10 M sodium thiosulfate solution. The rate expression for the reaction of Fe(VI) with DOX is represented by Equation (1):

$$r = -d[DOX]/dt = -k[ferrate(VI)]^a \cdot [DOX]^b \quad (1)$$

The reaction rate between Fe(VI) and DOX is represented by r , while k stands for the reaction rate constant. The parameters a and b in Equation (1) denote the reaction orders relating to the concentrations of Fe(VI) and DOX, respectively. It was widely reported that the oxidation of an organic contaminant by Fe(VI) follow second-order kinetics [18–20]. Therefore, Equation (1) can be reduced to Equation (2):

$$\ln\left(\frac{[DOX]_t}{[DOX]_0}\right) = -k_{app} \int_0^t [Fe(VI)] dt \quad (2)$$

where $[DOX]_t$ and $[DOX]_0$ are the concentrations of DOX at different reaction time, t and zero, respectively. All the samples were withdrawn and analyzed in triplicate.

2.5. Analytical Methods

2.5.1. The DOX Concentration

The DOX concentration was determined using high-performance liquid chromatography (HPLC) (Shimadzu, LC-20A), as referred to in the previous literature [21]. Under the conditions in Table S1, the characteristic peak of DOX appeared at about 3.9 min, and the calibration curve of DOX concentration is presented in Figure S2.

2.5.2. Identification of Oxidized Products

The intermediate products of DOX were characterized by GC–MS with the conditions in Table S1 (Shimadzu GCMS-QP2010plus, Kyoto, Japan), using parameters referenced previously [22]. All samples were acidified with hydrochloric acid to pH < 1 and concentrated by using a liquid–liquid method, extracted using trichloromethane.

2.6. Characterization

The specific surface area and porosity was carried out using ASAP 2460 devices (Micromeritics, Atlanta, GA, USA) by the Brunauer–Emmett–Teller (BET) and Barret–Joyner–Halender (BJH) methods. Fourier transform infrared (FTIR) spectra were measured by Nicolet iS20 devices (400–4000 cm⁻¹, Thermo Scientific, MA, USA).

3. Results and Discussion

3.1. DOX Removal by Fe(VI) Oxidation

3.1.1. The Impact of Fe(VI) Dosage

In this experiment, various quantities of Fe(VI) were introduced to a solution containing 11.25 µM DOX at pH 7.0, with the objective of removing it within 60 min. The result in Figure 1 showed that DOX removal increased from 82.47 to 96.98% as the molar ratio ([Fe(VI)]:[DOX]) increased from 5:1 to 30:1. This demonstrated that DOX was almost fully removed by Fe(VI) at a molar ratio of 30:1. This could be attributed to the increased probability of collisions between Fe(VI) and DOX molecules when increasing the Fe(VI)

dosage. In addition, the results showed that DOX removal can reach more than 70% within 5 min under all conditions. However, at lower Fe(VI) doses, DOX removal was quicker in the initial stages of the reaction, which might be attributed to its rapid self-decomposition (Equations (3) and (4)) as the Fe(VI) concentration increased [22]. This led to the ability of per unit Fe(VI) to remove DOX reduced [23].

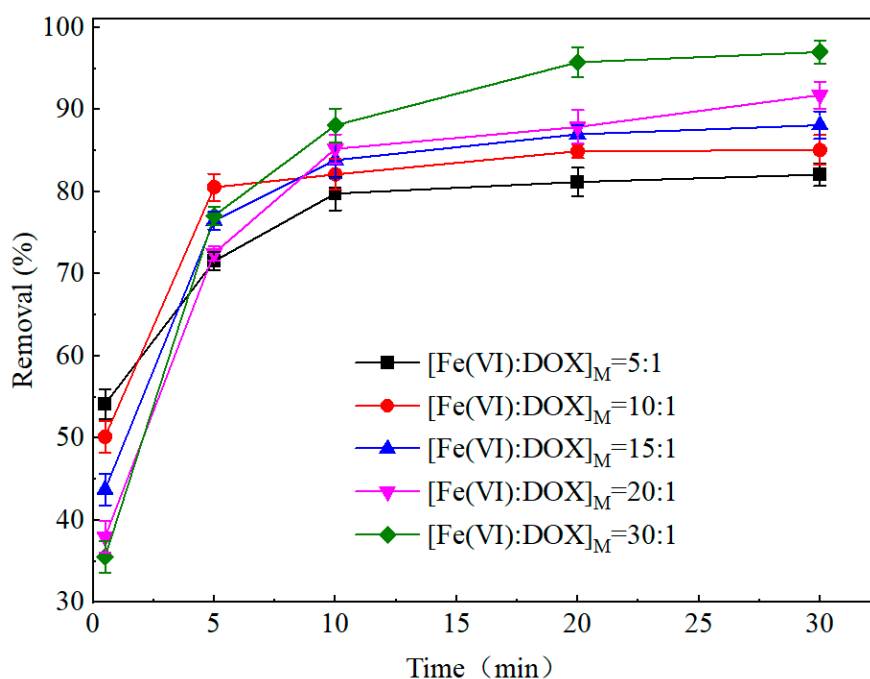
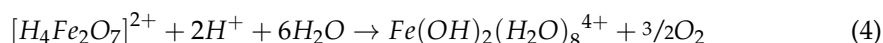
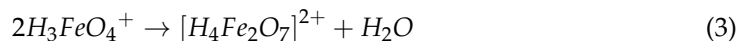


Figure 1. Effect of Fe(VI) dose on DOX degradation.

3.1.2. Impact of pH

Given that pH greatly influences the redox potential and stability of Fe(VI), the impact of pH on the removal of DOX by Fe(VI) was explored (Figure 2). In the experiment, the pH ranged from 4.0 to 10.0, the initial concentration of DOX was 11.25 μ M and the molar ratio ([Fe(VI)]:[DOX]) was set at 5:1. The reaction between DOX and Fe(VI) ended within 10 min, and DOX removal reached more than 80% under all pH conditions. With the increase in pH, DOX removal showed a tendency to decrease first and then rise. At pH 7.0, DOX removal was the lowest (80.92%), and reached its maximum at pH 9.0 (97.48%). DOX removal under the other pH conditions were 91.04 (pH 4.0), 88.53 (pH 5.0), 86.61 (pH 6.0), 95.12 (pH 8.0) and 93.01% (pH 10.0). The reaction rates between DOX and Fe(VI) gradually decreased as pH increased during the initial reaction period (within the first 2 min), but DOX removal by Fe(VI) was more efficient under alkaline conditions. This may attributed to the higher redox potential (+2.2 V) of Fe(VI) [15] under acidic conditions compared to alkaline conditions (0.72 eV). Another reasonable explanation of the decrease in the reaction rate under acid conditions with the increase in pH could be that it is due to the conversion of the protonated form of Fe(VI) ($HFeO_4^-$) to the less reactive deprotonated Fe(VI) species (FeO_4^{2-}) in alkaline conditions [24]. Moreover, the potential explanation for improved DOX removal at pH 9 could be due to the pH value being close to DOX's dissociation constant of 9.15 (Table S2) [25], causing the best DOX degradation effect at pH 9.

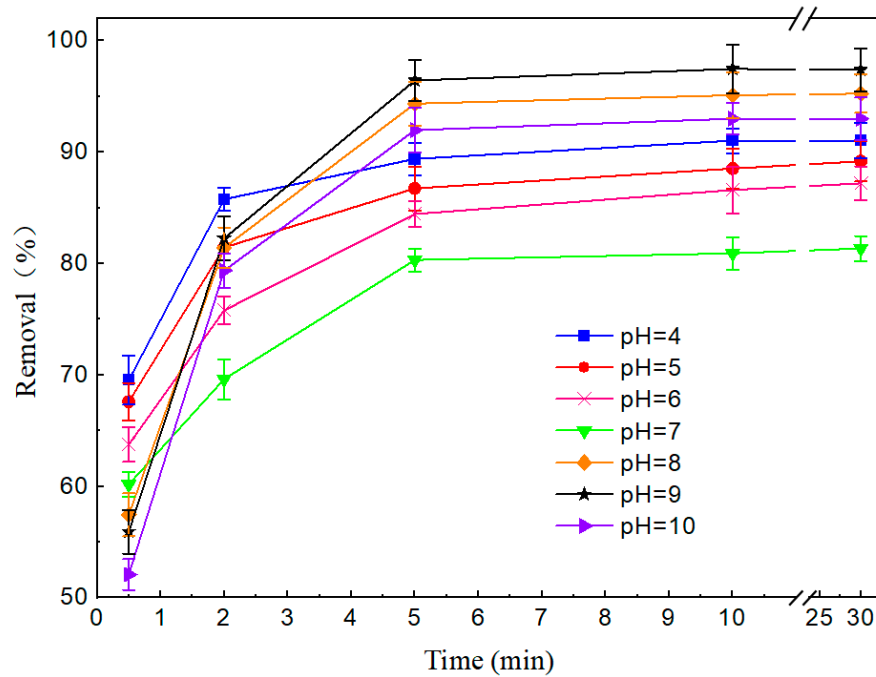


Figure 2. Effect of different pH values on DOX degradation.

3.1.3. Kinetics

Initially, the decline over time in both DOX and Fe(VI) in the reaction with excess Fe(VI) was determined at pH 7.0. The changes of Fe(VI) and DOX concentration over time with different dosage of Fe(VI) in Figure S3. The plots of $\ln([\text{DOX}]_t / [\text{DOX}]_0)$ versus $\int_0^t [\text{Fe(VI)}] dt$ are displayed in Figure 3. A linear relationship can be observed ($R^2 = 0.99$), indicating that the reaction of Fe(VI) with DOX followed second-order kinetics. The slope represents the second-order rate constant (k_{app}), which was $10.7 \pm 0.45 \text{ M}^{-1} \text{ s}^{-1}$.

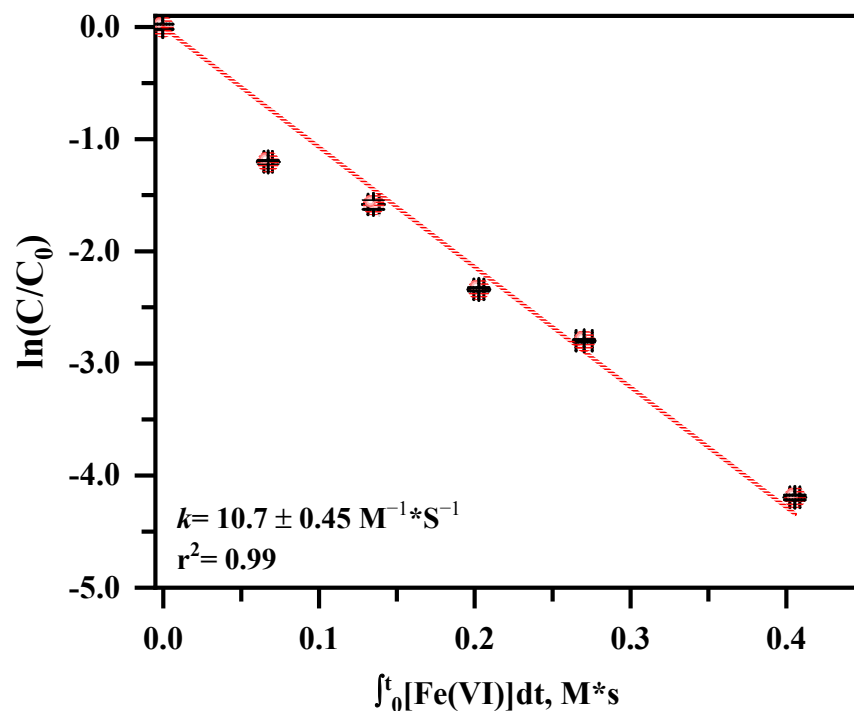


Figure 3. Kinetics analyses of DOX degradation by potassium Fe(VI).

3.1.4. Mineralization

In order to investigate the degradation degree of DOX by Fe(VI), the mineralization changes of DOX were recorded (Figure 4) [26–29]. The degradation of DOX reached a maximum within 5 min. At this time, DOX removal exceeded 77.0%, while TOC removal was only 39.2%. At 30 min, DOX removal reached 83%, while TOC removal in the solution barely increased. The results showed that, although Fe(VI) was able to remove DOX in a short time, it was limited in its ability eliminate DOX degradation products. Fe(VI) only oxidized DOX into other organic substances, and the mineralization degree was low. One study showed that that the mineralization efficiency of pristine Ag/AgCl and composites ACM-5 reached 18.97% and 46.65%, respectively, within 60 min [26]. Another study found that the transformation products of DOX with a small molecular weight were not observed even after 60 min of ozonation, suggesting that mineralization might be difficult [30]. Additionally, another study did not observe DOX degradation by peroxydisulfate oxidation [31]. The reasonable explanation for this may be that the structure of the naphthalene benzene ring in DOX is very stable and difficult to degrade, which is investigated further in Section 3.4.

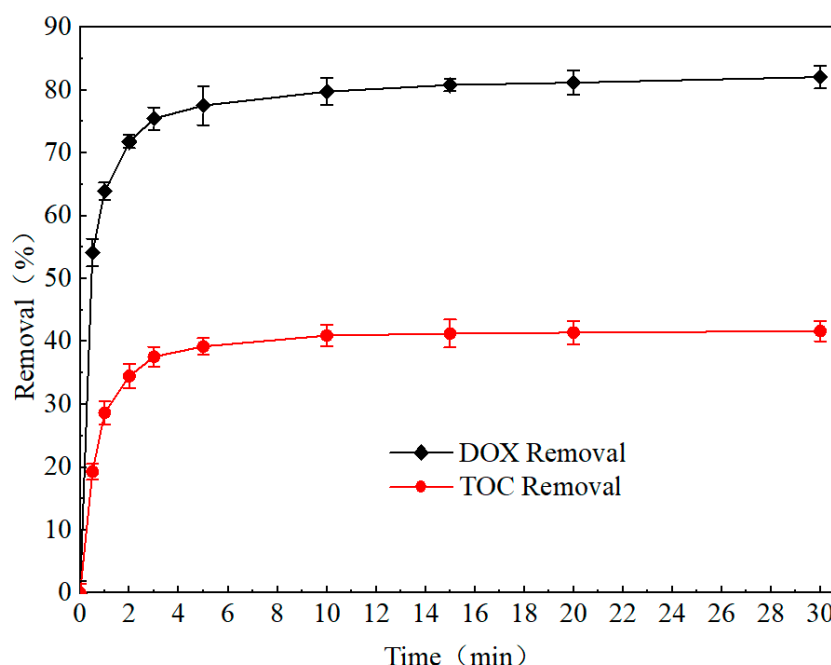


Figure 4. TOC and DOX removal at different reaction times.

3.2. Adsorption of DOX by Montmorillonite

3.2.1. Impact of Montmorillonite Dosage

To investigate the impact of montmorillonite dosage on DOX removal, different concentrations of montmorillonite were added to remove DOX in a solution at pH 7.0. The adsorption time was 24 h, with an initial DOX concentration of 11.25 μM . As the montmorillonite dosage increased from 100 to 600 mg/L, DOX removal by adsorption increased from 7.58 to 12.57%. Meanwhile, the absolute value of the zeta potential gradually increased from 15 to 27 mV, indicating that montmorillonite was stable and dispersed in the solution, resulting in an increase in DOX adsorption (Figure 5).

3.2.2. Impact of pH

In order to explore the effect of pH on the DOX adsorption efficiency by montmorillonite, the initial pH of the experimental solution was set at 2, 4, 6, 7, 8 and 10. All experiments were conducted at room temperature, the reaction time was 24 h, the initial concentration of DOX was 5 mg/L and the concentration of montmorillonite was 100 mg/L. With the increase in pH from 2.0 to 10.0, DOX removal decreased (Figure 6).

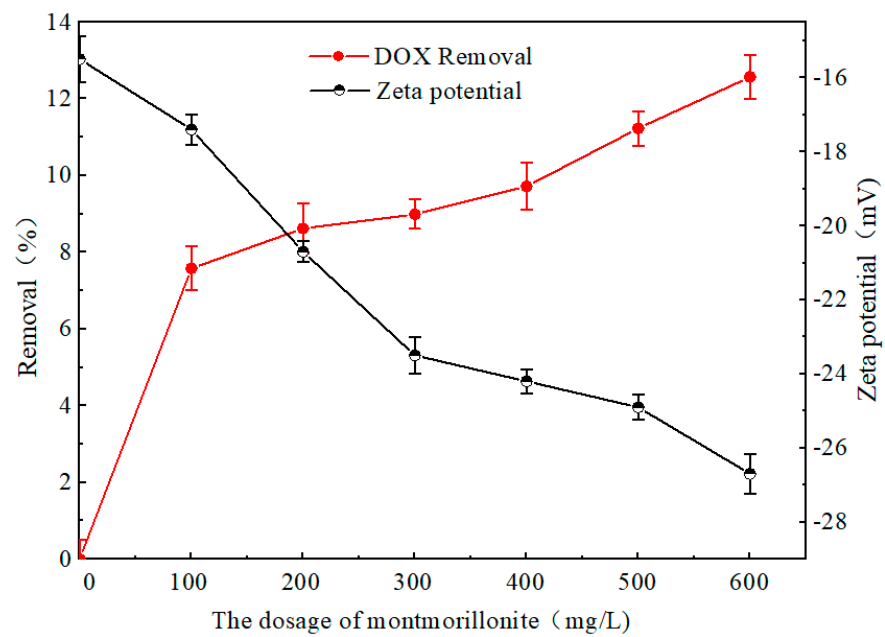


Figure 5. Effect of different dosages of montmorillonite on DOX removal.

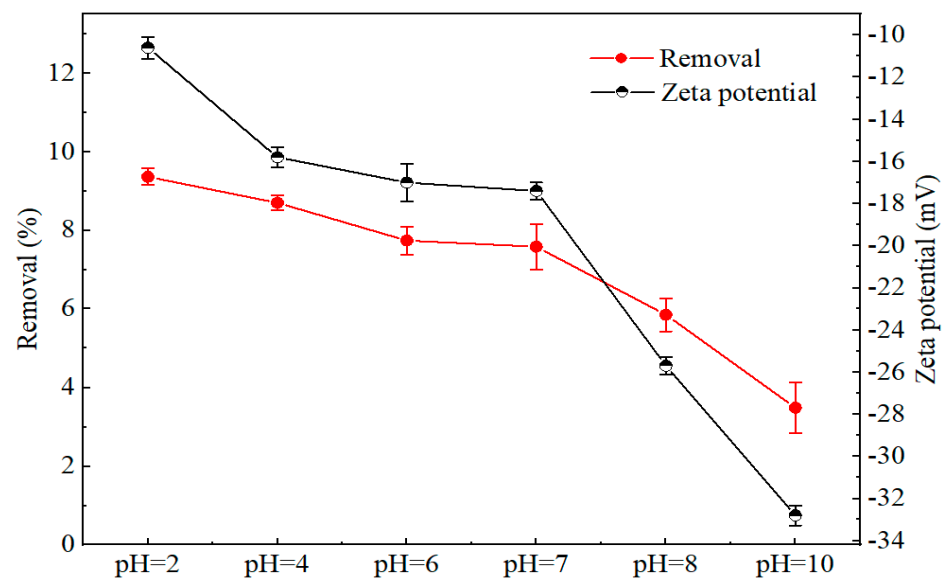


Figure 6. Effect of different pH values of montmorillonite on DOX removal.

Montmorillonite had the best effect on DOX removal (9.36%) at pH 7.0. Its removal under different pH conditions were: 8.7 (pH 4.0), 7.74 (pH 6.0), 7.58 (pH 7.0), 5.85 (pH 8.0) and 3.49% (pH 10.0). The adsorption of DOX by montmorillonite under acidic conditions was significantly higher than under alkaline conditions. For this result, one reasonable explanation is that the adsorption of DOX is influenced by DOX dissociation ($pK_{a1} = 3.02$, $pK_{a2} = 7.97$ and $pK_{a3} = 9.15$) [25]. The dominant species of DOX was ionized DOX^+ at pH 3.0. Concurrently, the zeta potential of the solution containing montmorillonite was negative, indicating that DOX could have been adsorbed via charge neutralization on the negatively charged surface of montmorillonite. Therefore, DOX adsorption by montmorillonite was the highest at pH 2. However, the dominant DOX species gradually turned from ionized DOX^+ to deprotonated DOX^- or DOX^{2-} as pH increased and the Zeta potential of montmorillonite surface become more negative (Figure 6) [32]. On account of the principle of heterogeneous charge repulsion, DOX adsorption by montmorillonite gradually decreased.

3.2.3. Impact of Adsorption Time

Adsorption time is one of the main factors affecting adsorption efficiency. In this experiment, 100 mg/L of montmorillonite was placed into a solution containing DOX (5 mg/L, 11.25 μ M) at pH 7.0. Additionally, samples at predetermined times—0, 0.5, 1, 2, 4, 6, 10, 12, 14, 18 and 24 h—were analyzed (Figure 7).

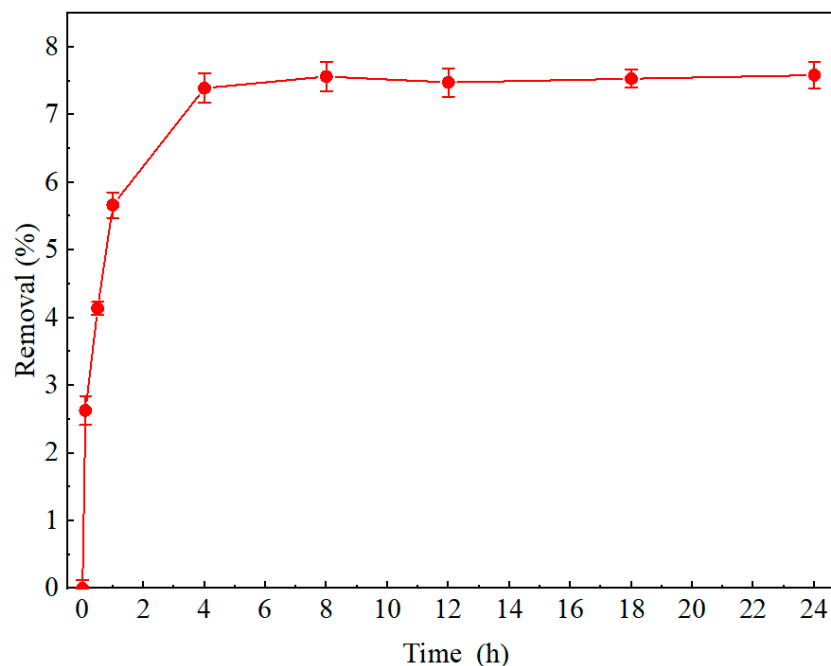


Figure 7. Effect of time on DOX removal by montmorillonite.

DOX adsorption by montmorillonite reached an equilibrium at 4 h, and the adsorption efficiency was very high in the early stages. The adsorption efficiency at 10 min was 2.63%, and with the extension of the adsorption time, the adsorption efficiency gradually increased to 4.14% at 30 min, 5.66% after 1 h and then 7.39% at 4 h. Afterwards, although the DOX concentration in the solution fluctuated slightly, it remained roughly unchanged. Therefore, there were two adsorption stages of DOX by montmorillonite, namely, an early rapid adsorption stage (0~4 h) and a later slow adsorption stage (4~24 h).

3.2.4. Effect of Adsorption Temperature

As temperature strongly affects adsorption, the influence of temperature on DOX adsorption by montmorillonite was investigated (Figure 8). In this study, 100 mg/L of montmorillonite was added to a solution containing DOX with concentrations ranging from 11.25 μ M to 675.01 μ M at pH 7. When the initial DOX concentration increased to 337.51 μ M, adsorption equilibriums at different temperatures were observed: 20.38 (25 $^{\circ}$ C), 26.40 (35 $^{\circ}$ C) and 29.43 mg/g (45 $^{\circ}$ C), indicating that the temperature increase was beneficial to DOX adsorption by montmorillonite. The reason for this result may be that the ionized DOX⁻ under neutral conditions was predominantly adsorbed by montmorillonite via van der Waals forces, which increased with faster molecular diffusion following a temperature rise [33].

3.3. Removal of DOX by Fe(VI) and Montmorillonite

To investigate the synergistic effect of oxidation and adsorption, Fe(VI) and montmorillonite were dosed in three different sequences under neutral conditions: (i) oxidation first and adsorption; (ii) adsorption first and then oxidation; (iii) simultaneous oxidation and adsorption. The above experimental results are shown in Figure 9. Additionally, the results of DOX removal by Fe(VI) and montmorillonite alone at pH 7.0 are shown

in Figure 10. At pH 7.0, DOX removal (5 mg/L, 11.25 μM) by Fe(VI) with a molar ratio of 5:1 ([Fe(VI)]:[DOX]) was 82.07% after 60 min. Under the same experimental conditions, DOX adsorption by 100 mg/L montmorillonite after adsorption for 24 h was 7.58% (Figure S4).

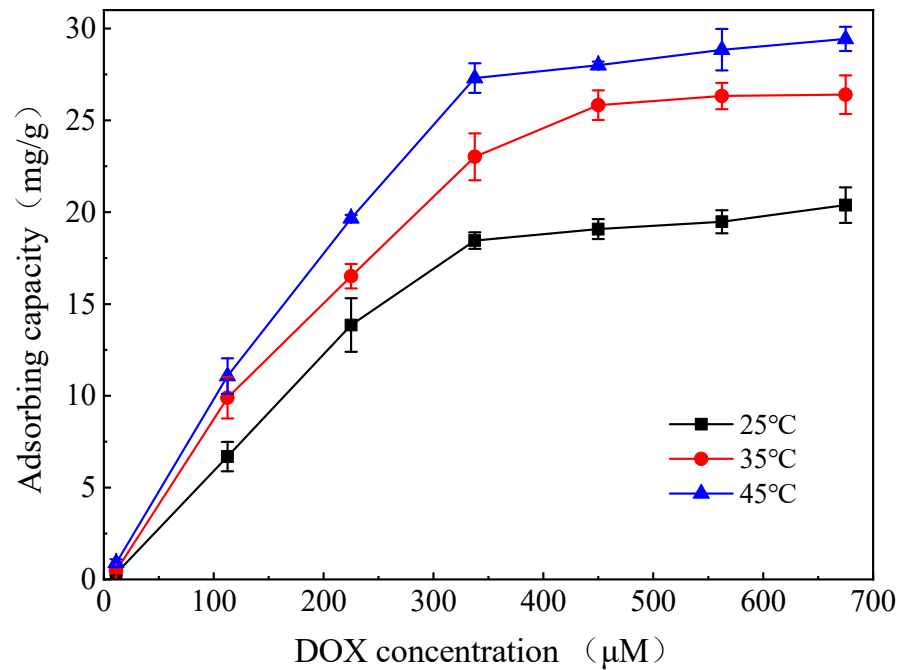


Figure 8. Effect of temperature on DOX removal by montmorillonite.

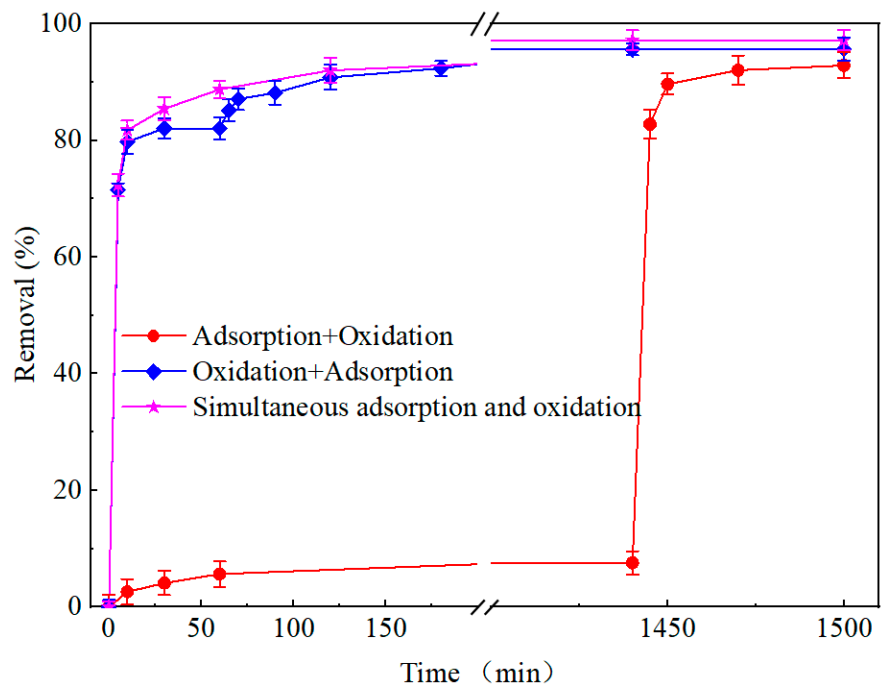


Figure 9. Comparison of different dosing sequences of Fe(VI) and montmorillonite on DOX removal.

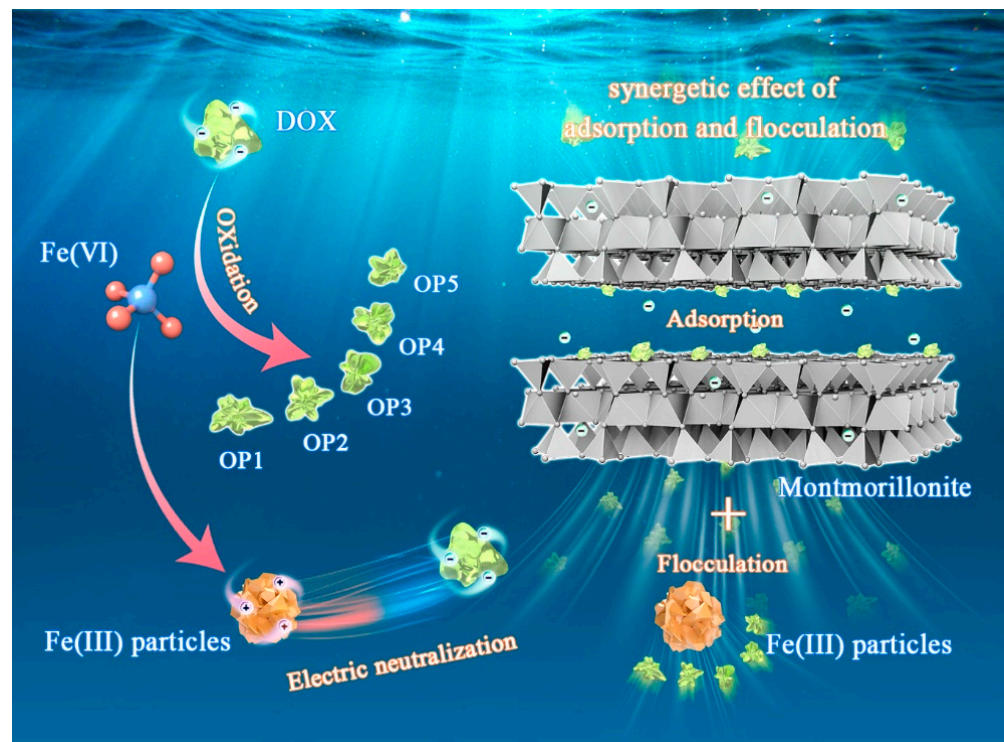


Figure 10. The synergy mechanism of DOX removal by Fe(VI) and montmorillonite.

The results of many experiments showed that DOX removal can be improved by combining Fe(VI) with montmorillonite. The synergy mechanism is shown in Figure 10. All three dosing sequences (Fe(VI) oxidation first and then adsorption, adsorption first and then Fe(VI) oxidation, simultaneous oxidation with adsorption) contribute to DOX removal (Figure 9). The optimal DOX removal efficiency (97.18%) was obtained under the synergetic effect of simultaneous Fe(VI) oxidation and montmorillonite adsorption. There may be two reasonable explanations for this. First, the highly positively charged intermediate product generated during Fe(VI) decomposition was neutralized with negatively charged montmorillonite. Additionally, the oxidation characteristics of Fe(VI) made DOX react with parts of the organic surface coating of colloidal particles, thus breaking through the organic coating, enhancing the electric neutralization of Fe(OH)₃ coagulants and colloidal particles [34]. This may reduce the repulsion between particles and enable larger flocs to agglomerate, improving the settling performance of flocs and the turbidity removal effect. Secondly, in the simultaneous adsorption experiment, montmorillonite not only adsorbed DOX and its degradation products, but it can also promote adsorption bridging, net flapping and sweeping and electric neutralization with negatively charged in situ Fe(III) particles, enhancing adsorption and flocculation. Furthermore, the turbidity caused by montmorillonite can be settled by Fe(III) flocculation.

3.4. Characterization of Fe(III)-Montmorillonite Composite and Montmorillonite

In order to evaluate the pore characteristic (specific surface, pore volume and pore size) of the Fe(VI)-montmorillonite composite, N₂ adsorption–desorption analysis was performed. Consistent with the IUPAC classification [35], both Fe(III)-montmorillonite composite and montmorillonite showed Type IVa isotherm pattern with a significant H3 type hysteresis loop (Figure S5), indicating the presence of mesopores [36], this can also be seen from BJH adsorption dV/dD pore volume (Figure S6). Due to the existence of the hysteresis curve, the pores are corrugated, resilient and expansible [37]. The Fe(III)-montmorillonite composite and montmorillonite surfaces were analyzed with a scanning electron microscope (SEM) and a transmission electron microscope (TEM). The results showed that montmorillonite has a layered structure (Figure S7a); after being combined

with Fe(III) particles, it presents a non-geometric shape (Figure S7b,c), which indicated that Fe(III) and montmorillonite were successfully combined.

The BET surface area and BJH pore size of montmorillonite were 159.33 m²/g and 6.42 nm, respectively. Comparatively, the Fe(III)-montmorillonite composite had a higher BET surface area and BJH pore size (195.37 m²/g and 5.98 nm) (Figure S6 and Table S4), indicating the coordination of Fe(III) particle and montmorillonite promoted the adsorption capacity of sole montmorillonite. This result validated the synergistic effect of Fe(VI) and montmorillonite combination on DOX removal, due to the enhanced adsorption by formation of Fe(III)-montmorillonite composite.

3.5. Plausible DOX Degradation Pathway

GC-MS was used to identify the five intermediates of DOX when oxidized by Fe(VI). The degradation products detected at each reaction period are shown in Table S3 and Figure S8. Referring to the measured m/z value, the previous literature and considering the molecular structure of the target pollutants with the oxidation characteristics of Fe(VI) [30,31,38,39], the possible degradation pathway of DOX is proposed in Figure 11. The molecular structure of DOX contains a stable naphthol ring, so when Fe(VI) oxidizes DOX it predominantly attacks the hydroxyl, amino and methyl groups in the DOX structure. Combined with the TOC degradation results, it can be seen that it is difficult for Fe(VI) to open the naphthol ring and oxidize DOX into small molecules. From the TOC degradation effect of DOX (41.68%), it can be noted that, while the degradation efficiency of DOX by Fe(VI) was high, the degree of oxidation mineralization was insignificant, similar to previous research results concerning tetracycline hydrochloride removal by Fe(VI) [29,40,41]. As seen in Figure 10, when oxidized by Fe(VI), the phenolic hydroxyl groups and hydroxyl groups on the naphthol ring of DOX are first oxidized, and the phenolic hydroxyl groups are broken and oxidized into p-benzoquinone, while the C–O bond on the naphthol ring is broken, losing two hydroxyl groups to generate the intermediate product OP1. Subsequently, one C–N bond on the naphthol ring of OP1 is broken, losing one amino group and turning into a carboxyl group, while the other two C–N bonds break and lose two methyl groups to produce the intermediate OP2. Later, the intermediate OP2 continues to be oxidized, resulting in C–C bond breaking and the loss of a carboxyl group to form the intermediate OP3. At this point, the p-benzoquinone structure on the naphthol ring continues to lose one H₂C=CH₂ bond due to the oxidation of Fe(VI), producing the intermediate product OP4. Finally, OP4 continues to be oxidized, losing two carboxyl groups, and becomes OP5, the final product of DOX oxidation.

The FTIR band is captured for Fe(III)-montmorillonite at 400–4000 cm⁻¹, the FTIR spectra were performed to reveal the nature of the interfacial interactions between interlayers of Fe(III)-montmorillonite composite and montmorillonite after reaction (Figure 12). The bands located at 1043 cm⁻¹ are assigned to NO₃⁻ symmetry stretching [42,43]. The spectrum also shows stretching modes at 3434 cm⁻¹ [43], while the bending modes appear at 1635 cm⁻¹ [44]. These samples show evidence for the presence of NH₃⁺ [44]. It proves that the C–N bond on the naphthol ring of OP1 was broken, losing one amino group, and parts of them were oxidized to NO₃⁻ by Fe(VI).

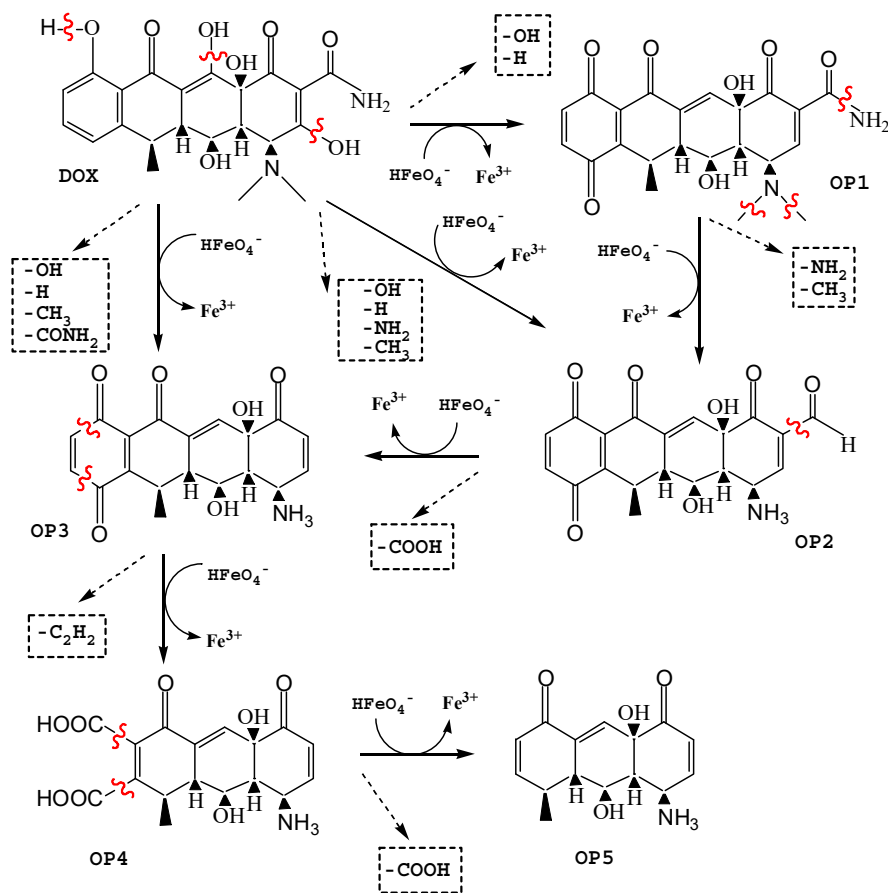


Figure 11. Proposed pathway of DOX degradation by Fe(VI).

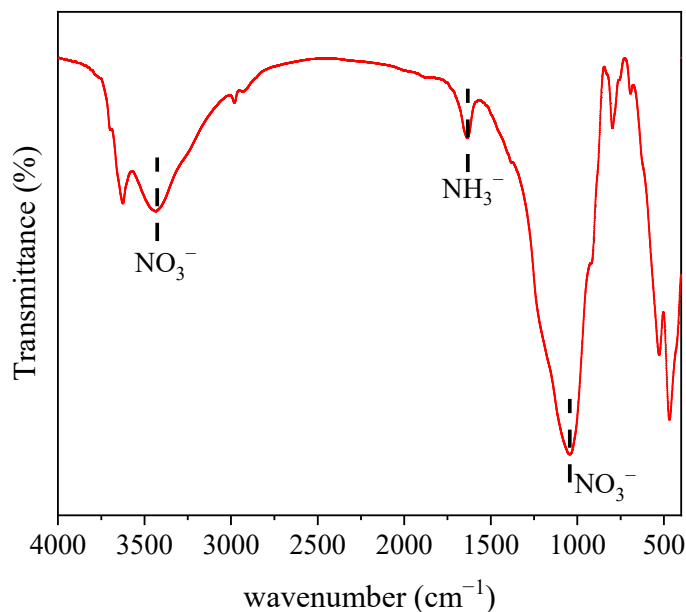


Figure 12. FTIR spectra for the Fe(III) + montmorillonite composite.

4. Conclusions

Fe(VI) is highly oxidizing and DOX removal can be effectively improved by the incremental dosage of Fe(VI) and montmorillonite. Under acidic conditions, DOX oxidation by Fe(VI) and the adsorption of DOX by montmorillonite can be promoted in the initial reaction stage. The oxidation of DOX by Fe(VI) finishes within 30 min at an optimal pH of 9.

The adsorption of DOX by montmorillonite reaches an equilibrium at 4 h, and an increase in temperature promotes adsorption. In addition, DOX oxidation reactions by Fe(VI) follow second-order kinetics. Due to the stability of the structure of DOX, Fe(VI) cannot completely mineralize it. Although DOX was completely removed by Fe(VI), adding a small amount of montmorillonite to the system can promote the further degradation of DOX (DOX removal increased from 82.07 to 97.18%). The removal rate was observed to be higher than simple oxidation. For example, 82% of DOX was removed by the electrochemically generated Fe(VI) at the molar ratio of 5:1 [18]. The degradation ratios of DOX in the carbon black-activated peroxydisulfate and manganese–cobalt–tungsten composite oxidation process reached 87 and 80%, which was lower than Fe(VI)-montmorillonite synergetic system [31,38]. This indicated that the Fe(VI)-montmorillonite synergetic system was an efficient approach to the removal of DOX. In addition to the excellent degradation rate, the in situ Fe(III) particles formed by Fe(VI) decomposition acted as a good coagulant and flocculant, promoting the flocculation and precipitation of particles in solution, removing turbidity. Overall, this work demonstrates that DOX was almost eliminated via the synergy of Fe(VI) and montmorillonite, and provides insight into the combination of oxidants and adsorbents in water treatment.

Supplementary Materials: The following supporting information can be downloaded at: <https://www.mdpi.com/article/10.3390/w15091758/s1>, Text S1. The Fe(VI) determination by ABTS method; Figure S1: The recovery rate after filtering by 0.22 μm membrane; Figure S2: The standard curve of DOX; Figure S3: Concentration of Fe(VI) (a) and DOX (b) with the reaction time; Figure S4: Comparison of oxidation alone (left axis) and adsorption alone (right axis) on DOX removal; Figure S5: Isotherm Linear Plot: Montmorillonite (a), Fe(III)+montmorillonite (b); Figure S6: BJH Adsorption dV/dD Pore Volume; Figure S7: (a) SEM-montmorillonite; (b) SEM-Fe(III) with montmorillonite; (c) TEM-Fe(III)-montmorillonite particles; Figure S8: GC-MS spectra of DOX degraded (a) 5 min intermediates; (b) 30 min intermediates; (c) 45min intermediates; (d) 60 min intermediates; Table S1: The UPLC and GC-MS conditions; Table S2: Dissociation constants (pKa) of doxycycline [25,32]; Table S3: Detection products in DOX degradation by GC-MS; Table S4. Textural attributes of adsorbents.

Author Contributions: Conceptualization, H.Z.; methodology, H.Z. and S.W.; software, H.Z. and S.W.; validation, H.W.; formal analysis, J.S.; investigation, S.W. and H.Z.; data curation, S.W. and H.Z.; writing—original draft, H.Z. and S.W.; writing—review and editing, H.Z. and J.S.; visualization, S.W. and H.Z.; supervision, H.W.; project administration, H.W.; funding acquisition, H.W. and H.Z. All authors have read and agreed to the published version of the manuscript.

Funding: The authors express their gratitude to the National Natural Science Foundation of China (Grant Numbers: 22178323) and the Basic Scientific Research Business Fees of Provincial Colleges and Universities (grant number: FRF22QN004) for their financial support in conducting this work.

Data Availability Statement: Data is contained within the article or supplementary material. The data presented in this study are available in Supplementary Materials.

Conflicts of Interest: The authors declare no conflict of interest.

References

1. Cheng, Y.; Ding, T.; Qian, Y.; Li, M.; Li, J. Advances in Biodegradation of Pharmaceuticals and Personal Care Products. *Sheng Wu Gong Cheng Xue Bao* **2019**, *35*, 2151–2164. [PubMed]
2. Akinbowale, O.L.; Peng, H.; Barton, M.D. Diversity of Tetracycline Resistance Genes in Bacteria from Aquaculture Sources in Australia. *J. Appl. Microbiol.* **2007**, *103*, 2016–2025. [CrossRef] [PubMed]
3. Comeau, F.; Surette, C.; Brun, G.L.; Losier, R. The Occurrence of Acidic Drugs and Caffeine in Sewage Effluents and Receiving Waters from Three Coastal Watersheds in Atlantic Canada. *Sci. Total Environ.* **2008**, *396*, 132–146. [CrossRef] [PubMed]
4. Lishman, L.; Smyth, S.A.; Sarafin, K.; Kleywegt, S.; Toito, J.; Peart, T.; Lee, B.; Servos, M.; Beland, M.; Seto, P. Occurrence and Reductions of Pharmaceuticals and Personal Care Products and Estrogens by Municipal Wastewater Treatment Plants in Ontario, Canada. *Sci. Total Environ.* **2006**, *367*, 544–558. [CrossRef] [PubMed]
5. Wang, L.; Ying, G.G.; Zhao, J.L.; Yang, X.B.; Chen, F.; Tao, R.; Liu, S.; Zhou, L.J. Occurrence and Risk Assessment of Acidic Pharmaceuticals in the Yellow River, Hai River and Liao River of North China. *Sci. Total Environ.* **2010**, *408*, 3139–3147. [CrossRef]
6. Goswami, R.K.; Agrawal, K.; Verma, P. An Exploration of Natural Synergy Using Microalgae for the Remediation of Pharmaceuticals and Xenobiotics in Wastewater. *Algal Res.* **2022**, *64*, 102703. [CrossRef]

7. Hanna, N.; Sun, P.; Sun, Q.; Li, X.; Yang, X.; Ji, X.; Zou, H.; Ottoson, J.; Nilsson, L.E.; Berglund, B.; et al. Presence of Antibiotic Residues in Various Environmental Compartments of Shandong Province in Eastern China: Its Potential for Resistance Development and Ecological and Human Risk. *Environ. Int.* **2018**, *114*, 131–142. [[CrossRef](#)]
8. Ma, J.; Wang, Z.; Zhang, Z.; Liu, Q.; Li, L. Distribution Characteristics of 29 Antibiotics in Groundwater in Harbi. *Rock Miner. Anal.* **2021**, *40*, 944–953.
9. Rahman, N.; Raheem, A. Graphene Oxide/Mg-Zn-Al Layered Double Hydroxide for Efficient Removal of Doxycycline from Water: Taguchi Approach for Optimization. *J. Mol. Liq.* **2022**, *354*, 118899. [[CrossRef](#)]
10. Gatica, J.; Cytryn, E. Impact of Treated Wastewater Irrigation on Antibiotic Resistance in the Soil Microbiome. *Environ. Sci. Pollut. Res.* **2013**, *20*, 3529–3538. [[CrossRef](#)]
11. Wang, D.; Zeng, Z.; Zhang, H.; Zhang, J.; Bai, R. How Does PH Influence Ferrate(VI) Oxidation of Fluoroquinolone Antibiotics? *Chem. Eng. J.* **2022**, *431*, 133381. [[CrossRef](#)]
12. Acosta-Rangel, A.; Sánchez-Polo, M.; Rozalen, M.; Rivera-Utrilla, J.; Polo, A.M.S.; Berber-Mendoza, M.S.; López-Ramón, M.V. Oxidation of Sulfonamides by Ferrate(VI): Reaction Kinetics, Transformation Byproducts and Toxicity Assesment. *J. Environ. Manag.* **2020**, *255*, 109927. [[CrossRef](#)] [[PubMed](#)]
13. Shu, J.; Wang, K.; Sharma, V.K.; Xu, X.; Nesnas, N.; Wang, H. Efficient Micropollutants Degradation by Ferrate (VI)-Ti/Zn LDH Composite under Visible Light: Activation of Ferrate (VI) and Self-Formation of Fe (III) -LDH Heterojunction. *Chem. Eng. J.* **2023**, *456*, 141127. [[CrossRef](#)]
14. Lee, Y.; Zimmermann, S.G.; Kieu, A.T.; Von Gunten, U. Ferrate (Fe(VI)) Application for Municipal Wastewater Treatment: A Novel Process for Simultaneous Micropollutant Oxidation and Phosphate Removal. *Environ. Sci. Technol.* **2009**, *43*, 3831–3838. [[CrossRef](#)]
15. Sharma, V.K. Potassium Ferrate(VI): An Environmentally Friendly Oxidant. *Adv. Environ. Res.* **2002**, *6*, 143–156. [[CrossRef](#)]
16. Hörsing, M.; Ledin, A.; Grabic, R.; Fick, J.; Tysklind, M.; la Cour Jansen, J.; Andersen, H.R. Determination of Sorption of Seventy-Five Pharmaceuticals in Sewage Sludge. *Water Res.* **2011**, *45*, 4470–4482. [[CrossRef](#)]
17. Li, J.; Yin, C.; Ma, H.; Fen, X.; Cheng, G. Research Progress on Modification and Application of Montmorillonite. *Technol. Dev. Chem. Ind.* **2021**, *50*, 25–29.
18. Wang, K.M.; Shu, J.; Wang, S.J.; Hong, T.Y.; Xu, X.P.; Wang, H.Y. Efficient Electrochemical Generation of Ferrate(VI) by Iron Coil Anode Imposed with Square Alternating Current and Treatment of Antibiotics. *J. Hazard. Mater.* **2020**, *384*, 121458. [[CrossRef](#)]
19. Lee, Y.; Yoon, J.; Von Gunten, U. Spectrophotometric Determination of Ferrate (Fe(VI)) in Water by ABTS. *Water Res.* **2005**, *39*, 1946–1953. [[CrossRef](#)]
20. Yang, B.; Ying, G.G.; Zhang, L.J.; Zhou, L.J.; Liu, S.; Fang, Y.X. Kinetics Modeling and Reaction Mechanism of Ferrate(VI) Oxidation of Benzotriazoles. *Water Res.* **2011**, *45*, 2261–2269. [[CrossRef](#)]
21. Xu, N.; Dong, J.; Zhou, W.; Liu, Y.; Ai, X. Determination of Doxycycline, 4-Epidoxycycline, and 6-Epidoxycycline in Aquatic Animal Muscle Tissue by an Optimized Extraction Protocol and Ultra-Performance Performance Liquid Chromatography with Ultraviolet Detection. *Anal. Lett.* **2019**, *52*, 452–464. [[CrossRef](#)]
22. Wang, H.; Liu, Y.; Jiang, J.-Q. Reaction Kinetics and Oxidation Product Formation in the Degradation of Acetaminophen by Ferrate (VI). *Chemosphere* **2016**, *155*, 583–590. [[CrossRef](#)] [[PubMed](#)]
23. Feng, M.; Wang, X.; Chen, J.; Qu, R.; Sui, Y.; Leslie, C.; Wang, Z.; Sharma, V.K. Degradation of Fluoroquinolone Antibiotics by Ferrate(VI): Effects of Water Constituents and Oxidized Products. *Water Res.* **2016**, *103*, 48–57. [[CrossRef](#)] [[PubMed](#)]
24. Sharma, V.K.; Sohn, M.; Anquandah, G.A.K.; Nesnas, N. Kinetics of the Oxidation of Sucralose and Related Carbohydrates by Ferrate(VI). *Chemosphere* **2012**, *87*, 644–648. [[CrossRef](#)] [[PubMed](#)]
25. Qiang, Z.; Adams, C. Potentiometric Determination of Acid Dissociation Constants (PK a) for Human and Veterinary Antibiotics. *Water Res.* **2004**, *38*, 2874–2890. [[CrossRef](#)] [[PubMed](#)]
26. Wen, X.J.; Shen, C.H.; Niu, C.G.; Lai, D.C.; Zhu, M.S.; Sun, J.; Hu, Y.; Fei, Z.H. Attachment of Ag/AgCl Nanoparticles on CdMoO₄ Microspheres for Effective Degradation of Doxycycline under Visible Light Irradiation: Degradation Pathways and Mineralization Activity. *J. Mol. Liq.* **2019**, *288*, 111063. [[CrossRef](#)]
27. Wen, X.J.; Niu, C.G.; Zhang, L.; Liang, C.; Zeng, G.M. A Novel Ag₂O/CeO₂ Heterojunction Photocatalysts for Photocatalytic Degradation of Enrofloxacin: Possible Degradation Pathways, Mineralization Activity and an in Depth Mechanism Insight. *Appl. Catal. B Environ.* **2018**, *221*, 701–714. [[CrossRef](#)]
28. Zhi, D.; Wang, J.; Zhou, Y.; Luo, Z.; Sun, Y.; Wan, Z.; Luo, L.; Tsang, D.C.W.; Dionysiou, D.D. Development of Ozonation and Reactive Electrochemical Membrane Coupled Process: Enhanced Tetracycline Mineralization and Toxicity Reduction. *Chem. Eng. J.* **2020**, *383*, 123149. [[CrossRef](#)]
29. Dalmázio, I.; Almeida, M.O.; Augusti, R.; Alves, T.M.A. Monitoring the Degradation of Tetracycline by Ozone in Aqueous Medium Via Atmospheric Pressure Ionization Mass Spectrometry. *J. Am. Soc. Mass Spectrom.* **2007**, *18*, 679–686. [[CrossRef](#)]
30. Park, J.A.; Pineda, M.; Peyot, M.L.; Yargeau, V. Degradation of Oxytetracycline and Doxycycline by Ozonation: Degradation Pathways and Toxicity Assessment. *Sci. Total Environ.* **2023**, *856*, 159076. [[CrossRef](#)]
31. Chen, Y.; Yin, R.; Zeng, L.; Guo, W.; Zhu, M. Insight into the Effects of Hydroxyl Groups on the Rates and Pathways of Tetracycline Antibiotics Degradation in the Carbon Black Activated Peroxydisulfate Oxidation Process. *J. Hazard. Mater.* **2021**, *412*, 125256. [[CrossRef](#)] [[PubMed](#)]

32. Zhang, X.; Bai, B.; Li, G.; Wang, H.; Suo, Y. Novel Sea Buckthorn Biocarbon SBC@ β -FeOOH Composites: Efficient Removal of Doxycycline in Aqueous Solution in a Fixed-Bed through Synergistic Adsorption and Heterogeneous Fenton-like Reaction. *Chem. Eng. J.* **2016**, *284*, 698–707. [[CrossRef](#)]
33. Parsegian, V.A.; Ninham, B.W. *Temperature-Dependent Van Der Waals Forces*; Elsevier: Amsterdam, The Netherlands, 1970; Volume 10.
34. Ma, Y.; Gao, N.; Li, C. Degradation and Pathway of Tetracycline Hydrochloride in Aqueous Solution by Potassium Ferrate. *Environ. Eng. Sci.* **2012**, *29*, 357–362. [[CrossRef](#)]
35. Thommes, M.; Kaneko, K.; Neimark, A.V.; Olivier, J.P.; Rodriguez-Reinoso, F.; Rouquerol, J.; Sing, K.S.W. Physisorption of Gases, with Special Reference to the Evaluation of Surface Area and Pore Size Distribution (IUPAC Technical Report). *Pure Appl. Chem.* **2015**, *87*, 1051–1069. [[CrossRef](#)]
36. Li, B.; Zhao, Y.; Zhang, S.; Gao, W.; Wei, M. Visible-Light-Responsive Photocatalysts toward Water Oxidation Based on NiTi-Layered Double Hydroxide/Reduced Graphene Oxide Composite Materials. *ACS Appl. Mater. Interfaces* **2013**, *5*, 10233–10239. [[CrossRef](#)] [[PubMed](#)]
37. Xing, L.; Haddao, K.M.; Emami, N.; Nalchifard, F.; Hussain, W.; Jasem, H.; Dawood, A.H.; Toghraie, D.; Hekmatifar, M. Fabrication of HKUST-1/ZnO/SA Nanocomposite for Doxycycline and Naproxen Adsorption from Contaminated Water. *Sustain. Chem. Pharm.* **2022**, *29*, 100757. [[CrossRef](#)]
38. Luo, X.; You, Y.; Zhong, M.; Zhao, L.; Liu, Y.; Qiu, R.; Huang, Z. Green Synthesis of Manganese–Cobalt–Tungsten Composite Oxides for Degradation of Doxycycline via Efficient Activation of Peroxymonosulfate. *J. Hazard. Mater.* **2022**, *426*, 127803. [[CrossRef](#)] [[PubMed](#)]
39. Zhang, J.; Wu, H.; Zhang, D.; Zhang, L.; Zhu, C. Preparation of a Ruthenium-Modified Composite Electrode and Evaluation of the Degradation Process and Degradation Mechanism of Doxycycline at This Electrode. *J. Water Process Eng.* **2022**, *48*, 102904. [[CrossRef](#)]
40. Jiao, S.; Meng, S.; Yin, D.; Wang, L.; Chen, L. Aqueous Oxytetracycline Degradation and the Toxicity Change of Degradation Compounds in Photoirradiation Process. *J. Environ. Sci.* **2008**, *20*, 806–813. [[CrossRef](#)]
41. Jiao, S.; Zheng, S.; Yin, D.; Wang, L.; Chen, L. Aqueous Photolysis of Tetracycline and Toxicity of Photolytic Products to Luminescent Bacteria. *Chemosphere* **2008**, *73*, 377–382. [[CrossRef](#)]
42. Bei, W.; Junhua, J.; Ting, Z.; Zhonghui, L. Determination of Soluble Ions in Atmospheric Aerosol by FTIR. *J. Henan Mech. Electr. Eng. Coll.* **2010**, *18*, 15–17.
43. Socrates, G. *Infrared and Raman Characteristic Group Frequencies: Tables and Charts*; John Wiley & Sons, Inc.: Hoboken, NJ, USA, 2001; ISBN 978-0-470-09307-8.
44. Hakiri, R.; Ameer, I.; Abid, S.; Derbel, N. Synthesis, X-Ray Structural, Hirshfeld Surface Analysis, FTIR, MEP and NBO Analysis Using DFT Study of a 4-Chlorobenzylammonium Nitrate (C₇ClH₉N)⁺(NO₃)⁻. *J. Mol. Struct.* **2018**, *1164*, 486–492. [[CrossRef](#)]

Disclaimer/Publisher's Note: The statements, opinions and data contained in all publications are solely those of the individual author(s) and contributor(s) and not of MDPI and/or the editor(s). MDPI and/or the editor(s) disclaim responsibility for any injury to people or property resulting from any ideas, methods, instructions or products referred to in the content.